A Study Into the Accountability of Evaporation in the Mass Reduction of the Aral Sea

A dissertation submitted in partial fulfilment of the requirements for B.Sc. Honours Physics

A Study Into the Accountability of Evaporation in the Mass Reduction of the Aral Sea

A dissertation submitted in partial fulfilment of the requirements for B.Sc. Honours Physics

Daniel North

2015

N0477346

Contents

1. Abstract

This is an investigation into the reduction of the Aral Sea. Satellite images from Landsat mission were analysed with the aim of discovering the surface area of the Aral Sea between 1987 and 2014. A model estimating the configuration of the sea bed was produced, and data extrapolated from the images evaluating area, to calculate the decreasing volume of the Aral Sea between the given dates. Through use of temperature increase estimates, and average values of temperature and wind speed, the evaporation rate of the sea was approximated. Coupling this data with the area evaluation, the estimated loss of volume due to evaporation was calculated. These values were finally compared, displaying that the evaporated water was responsible for less than a quarter of the Aral's total volume loss. This was the expected result and further confirms that climate change is not entirely responsible for the perishing Aral, but yet another symptom of the extensive, poorly constructed irrigation in the region.

2. Introduction

Remote sensing is the process of observation and data collection of an object that is separated from the detection equipment by an arbitrary distance. While there are many forms of remote sensing, all of them fall into one of two categories; active and passive. A passive system measures the signal from an object, and selects only the information it requires. An active system creates its own signal, reflecting it off the object and measuring the return signal. [1]

Satellite imagery is a common example of a passive system, measuring the light from Earth. The potential of aerial photography was recognised as early as 1858, when Gaspare Tournachon, a French writer, took to the skies of Paris with a hot air balloon and a camera [2]. It wasn't until 1959 that satellite imagery was first utilised, with the orbital satellite Explorer 6. This was the first satellite to transmit images from orbit, and it was built to photograph the Earth's cloud coverage [3]. In July 1972, NASA launched the Earth Resources Technology Satellite, the first of the Landsat program, which was later renamed Landsat-1 [4].

2.1. Landsat

The Landsat program was initiated with the belief that satellite imagery would solve a substantial number of problems in environmental science. It was soon realised that while useful information could be obtained from the gathered data, there were "substantial difficulties to be overcome and considerable challenges to be met" [5]. However, since then scientists have viewed satellite imagery not as the solution, but as a tool to be used in conjunction with existing ground based evidence [1].

Satellite imaging has countless applications, within scientific research and everyday life. It can be used to track and predict weather patterns, a luxury of modern times; but also the weather at sea, which is crucial for ships [6]. Map based applications on mobile phones and computers use satellite images devoid of cloud cover for their interactive maps, a very useful tool for the general population. Government agencies such as the National Reconnaissance Office acknowledge that their own satellites that perform reconnaissance from orbit (the reconnaissance itself is classified however) [7]. Satellites are also used in the fight against forest fires, to track their spread and minimise the damage they cause [8].

In order to achieve global coverage, Landsat-1 utilised a near-polar sun-synchronous orbit. This meant that, it kept the same local time on each orbit, with 14 orbits per day and a descending equatorial crossing at 9:30AM. With the orbit at a 99° inclination toward the equator, the 15th orbit of each day (or the beginning of the following day) had advanced by 159km. This advance would cycle over 18 days (or 251 full orbits), ensuring full coverage of the Earth; this is known as the temporal resolution [9].

Landsat-1 was decommissioned in January 1978, outliving its design specifications by five years. Landsat-2 had been launched in January 1975 and continued operating until it's decommissioning in July 1983 due to yaw control failure. In March 1978, Landsat 3 was launched, but after 3 months its thermal band detector stopped transmitting, it was finally decommissioned in September 1983. Landsat 4 was launched July 1982, however it suffered several communications failures during operation, and stopped transmitting in 1993; it was used for telemetry until decommission in 2001. In March 1984 Landsat-5 was launched, it outlived its three year design and was finally decommissioned in December 2012, after over 28 years of transmission. In 1993 Landsat-6 failed to achieve orbit after launch, if it were not

Landsat-5, a large data gap would have been inevitable. Landsat-7 was launched April 1999 and Landsat-8 in February 2013, both are still transmitting data [4].

2.2. Science of Landsat

All of the Landsat satellites have kept the polar orbit basis, with Landsat-2 and 3 being identical to the first. Landsat-4,5,7 and 8 had slightly altered orbits, with 14.56 orbits a day and a temporal resolution of 16 days (or 233 full orbits). The Landsat-7 and 8 satellites also have an equatorial crossing of 10AM local time each [9].

The imaging instruments on board Landsat-1,2,3 included a Return Beam Vidicon (RBV) and a Multispectral Scanner (MSS). The RBVs were cameras that took snapshot images of the ground directly below them, taking a picture every 25 seconds; a continuous line of contiguous images. Landsat-1,2 used three RBVs, each with a different spectral band; where Landsat-3 only included two RBVs, which were both panchromatic. The MSS scanned the surface of Earth in strips, using an oscillating mirror that reflected the light into four detectors. It was able to perceive four spectral bands, with an additional thermal band in Landsat-3. The MSS continued onto Landsat-4,5 but the RBV was replaced by a Thematic Mapper (TM). The TM had a similar design to the MSS, however it scanned the surface in two directions, greatly improving the spatial resolution. Seven spectral bands were included in the TM [9].

Landsat-7 includes an Enhanced Thematic Mapper (ETM). The ETM is an improvement on the TM, with an improved spatial resolution and an additional panchromatic detector. Landsat-8 uses the Operational Land Imager (OLI) and the Thermal Infra-Red Scanner (TIRS). Unlike previous scanners, OLI does not utilise mirrors in the mapping of Earth; instead it uses long detector arrays that hold over 7000 detectors per spectral band, which produce images with less noise. The OLI uses nine spectral bands. The TIRS measures the current from excited electrons to build an image; the electrons are excited by two distinct IR spectral bands, this aids in differentiating between the temperature of Earth and the atmosphere [10].

Instrument	Spectral Bands (μm)	Spatial Resolution (m)
Multispectral RBV (Return Beam Vidicon)	0.475 - 0.575 (blue)	79
	0.580 - 0.680 (red)	79
	0.689 - 0.830 (near infra-red)	79
Panchromatic RBV	0.505 - 0.750 (panchromatic)	40
MSS (Multispectral Scanner)	0.500 - 0.600 (green)	79
	0.600 - 0.700 (red)	79
	0.700 - 0.800 (near infra-red)	79
	0.800 - 1.100 (near infra-red)	79
	10.400 - 12.600 (thermal)	237
TM (Thematic Mapper)	0.450 - 0.520 (blue)	30
	0.520 - 0.600 (green)	30
	0.630 - 0.690 (red)	30

Instrument	Spectral Bands (μm)	Spatial Resolution (m)
TM (Thematic Mapper)	0.760 - 0.900 (near infra-red)	30
	1.550 - 1.750 (mid infra-red)	30
	2.080 - 2.350 (mid infra-red)	30
	10.400 12.500 (thermal)	120
ETM (Enhanced Thematic Mapper)	0.450 - 0.520 (blue)	30
	0.520 - 0.600 (green)	30
	0.630 - 0.690 (red)	30
	0.760 - 0.900 (near infra-red)	30
	1.550 - 1.750 (mid infra-red)	30
	2.080 - 2.350 (mid infra-red)	30
	10.400 - 12.500 (thermal)	60
	0.520 - 0.900 (panchromatic)	15

Instrument	Spectral Bands (μm)	Spatial Resolution (m)
OLI (Operational Land Imager)	0.433 - 0.453 (deep blue)	30
	0.450 - 0.515 (blue)	30
	0.525 - 0.600 (green)	30
	0.630 - 0.680 (red)	30
	0.845-0.885 (near infra-red)	30
	1.560 - 1.660 (mid infra-red)	30
	2.100 - 2.300 (mid infra-red)	30
	0.500 - 0.680 (panchromatic)	15
	1.360 - 1.390 (mid infra-red)	30
TIRS (Thermal Infra-Red Scanner)	10.600 - 11.200 (thermal)	100
	11.500 - 12.500 (thermal)	100

Fig.2.1 – *The list of the major imaging instruments included on Landsat 1-8. Information on the spectral range they are able to detect and the spatial resolution of the detectors* [11].

Landsat has focused on several different spectral ranges, because terrain features on Earth's surface correlate to certain wavelength ranges; this enables a considerable amount of data to be retrieved and analysed. The visible spectrum is 390nm-700nm, and is measured primarily in red/blue/green bands. Near infra-red is reflected by healthy plant life, while mid infra-red can differentiate between wet and dry earth, and rocks that appear similar in other bands are often visibly different [11]. Almost all of the light between 1.35μm-1.4μm *(Fig.2.1)* is reflected by the atmosphere, therefore the ground is almost invisible, and only clouds are measurable [11]. Thermal data is highly valuable in studying how both land and water are used, and also in meteorology [12].

The deep blue band measured by OLI is also mostly reflected in the atmosphere by dust and water, and the obtained images are visually similar to that of the blue band, but with less clarity. However, when the blue band image is subtracted from that of deep blue,

coastlines, living plant life and particles in the air (such as smoke) become much clearer. Panchromatic instruments detect all of the wavelengths at once, so it behaves similar to black and white film. It is the sharpest of all the detectors and has highest resolution. The images of other detectors are combined with this for higher quality images in the desired spectrum [11].

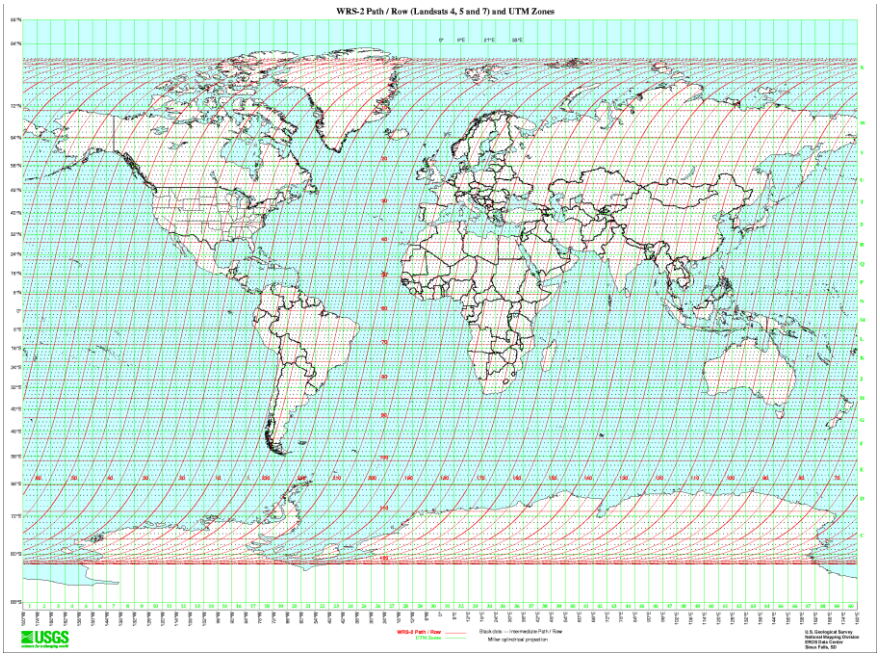

Fig.2.2 – *A diagram displaying the World Reference System. Red lines show WRS coordinates; horizontal lines are* ***Rows*** *and the* ***Passes*** *show Landsat's near polar orbit path as it advances.* [13]

Many satellite images aren't true colour, or don't include the entire visible spectrum; therefore they must be artificially coloured before they're released [14]. However, this is not the only image processing that satellite images require. Due to the Earths curvature, satellite images must be flattened to form a 2D map. Another issue is the satellites velocity and the Earth's rotation; this creates an offset in the image during the exposure time, the image must be straightened for a map to be formed [4]. Once the crucial image processing is completed, the images can be given coordinates, for a map to be constructed. The Landsat satellites adopt the World Reference System (and WRS-2 on Landsat-7,8), a coordinate system whose basis is Landsat's orbit trajectory, using "passes" and "rows" *(Fig.2.2)* [14]. This can then be translated into geographic coordinates [4].

The United States Geological Survey processes and publishes the Landsat data within 24 hours of its recording. It is then uploaded for anyone to use, free of charge [14]. This data is

further processed and/or studied by scientists around the world from many different fields. By combining the data from multiple detectors, a whole new set of data can be obtained. Many scientists have used the Landsat data to investigate the symptoms of climate change; such as detecting the effect of climate change on ecosystems in Romanian forests [15], and calculating the decrease in snow cover at Mount Kilimanjaro [16].

2.3. The Aral Sea

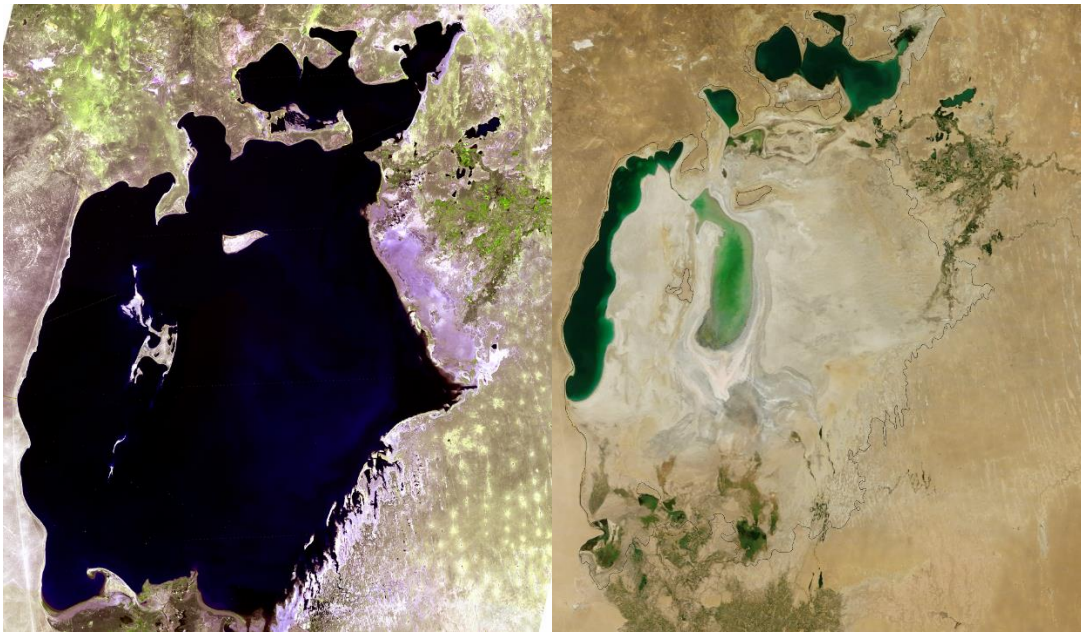

Fig.2.3 *– Two images of the Aral Sea. First taken in 1977 [17], second in 2011 [18].*

Central Asia has been greatly affected by climate change, in part caused by the rapid reduction in the size of the Aral Sea. The Aral Sea has declined to 10% of its original volume in the past 50 years. This has caused the local (and to a lesser extent regional) climate to become "more extreme, with hotter and drier summers and colder and longer winters" [19]. The Aral Sea once had a surface area of 68,000 km^2, one of the largest lakes in the world, but after Joseph Stalin proposed The Great Plan For The Transformation Of Nature, in which several reservoirs were built around Soviet Europe to ensure high crop yield, the sea began to diminish [19]. It is now composed of four smaller lakes. As part of his plan, during the early 1960s the USSR diverted the Amu Darya and the Syr Darya, the two rivers that fed the Aral Sea, in an attempt to increase crop yields in Uzbekistan [20].

Irrigation is not an inherently bad concept; it is used throughout the world on large and small scales to help crop growth and feed water to areas of low rainfall. Unfortunately, there are serious adverse effects that can occur if the circumstances change. Irrigation causes reduction in river flow, elevated water level within the water table (due to increased groundwater) and increased evaporation in the surrounding area (through larger surface area of water and larger concentrations of plant life). The reduced flow downstream can lead to the disappearance of essential wetlands, loss of aquatic life, and reductions in water for drinking and other uses. An increased volume of water within the water table can cause problems such as waterlogging to arise, which in turn cause floods, crop death (due to lack of air) and house water borne diseases [40].

A major contributor to the ruinous scenario is the sheer volume of water that is taken. The Karakum Canal drains 13km^3 from the Amu Darya river each year, or 25% of the river's water [21]. The reason such a volume is diverted is due to the poor construction of the canal (as most canals in the region are); it is estimated that 50% of the water escapes the canal through ground absorption and evaporation. Only 12% of Uzbekistan's canal is waterproofed. The water also escapes by other means, creating several lakes and ponds along the length of these canals. These have expedited the ground water in the surrounding areas, leading to severe ground salinization, where only 50% of crops can survive in the soil [21].

A toxic desert of chemicals and salt flats, scattered with the remains of boats and little vegetation, now occupies the basin of the Aral Sea. After years of acute climate change, biocide damage and even weapons testing, the remnants have become a hazardous area. The health problems in the area are also increasing, with high infant mortality rates (7.5%) and numerous diseases; stemming from toxic dust and little access to fresh, clean water [23].

The environmental impact caused by the reduction of the Aral Sea is a crisis that is escalating in severity. According to some scientists, the local effect coupled with global warming will increase the local temperature by 3.5°C by 2030, furthering the evaporation of the sea [23]. Efforts to aid the situation have been made, such as the restoration of the northern lake through dooming the southern lake, building a concrete dam to separate the two seas. The northern lake has received a significant rise. However, much of the damage done will not be easily corrected, if at all.

2.4. Objectives

This investigation aims to use the past 30 years of satellite imagery available, from Landsat, to re-gauge the rate at which the Aral Sea recedes through time. This data can then be used to calculate the volume of water that was removed from the Aral Sea over an arbitrary timeframe. Using the available data from past investigations, the temperature over these years can be acquired, then by using seasonal averages of ground temperature, the theoretical value for water evaporation over the Aral's surface can be estimated. Then with the calculated evaporation rate, a comparison to the observational decrease will be inspected. These will expectedly return different values, as the Aral has not disappeared solely through the evaporation from climate change. Through the results obtained, a conclusion to the cause of the remaining loss can be established.

3. Data Selection

The only source of satellite imagery in this investigation is the Landsat program. Therefore, to ensure a wide sample of data, images from all seven successful Landsat missions were inspected. This gives a maximum of 42 years of imagery; however only data from Landsat 4, 5, 7 & 8 was utilised, with 27 years of data between 1987 and 2014. All images were viewed using the USGS Earth Explorer [24] website, to determine their suitability, and downloaded via their Bulk Download Application.

3.1. Image Usability

Due to the vast size of the Aral Sea, it is never contained within a single [Landsat] image. Consequently multiple images of the Aral must be downloaded to process the data; however it takes 18 days for the satellite to photograph the entire Earth. This will cause fluctuations in the surface area of the Aral, with the sea out of alignment between images. Careful consideration of each image was needed, as this could be a large source of error. Each of the images used were either in alignment, or possessed a minimal difference that was considered negligible; the water had only "relocated" to another shore on the sea during tidal changes.

This is not the only obstacle involved with the selection of Landsat images; the largest problem is cloud cover. While attempting to measure the area of a feature such as this, cloud cover obscuring the image is unacceptable (see Fig.4). While processes to remove clouds with in the sea (such as taking the coastline and measuring its interior) can be utilised, any cloud that blurs the coastline will result in imprecise measurements. The Earth Explorer tool allows images with cloud cover to be filtered out of results; all images obtained contain less than 10% cloud coverage.

Additionally Landsat imagery uses false colour images, as each camera is finely tuned to a small waveband. Due to the false colour being used, the water in this scene (see Fig.3.1) is taken from the reflectance of all visible light, and coloured blue, giving the clouds a bright turquoise colour. This colour is similar to that of the shallow high salinity waters parts of the Aral possess, and can be unnoticeable at first, giving the sea a larger area as they stray over the coast lines.

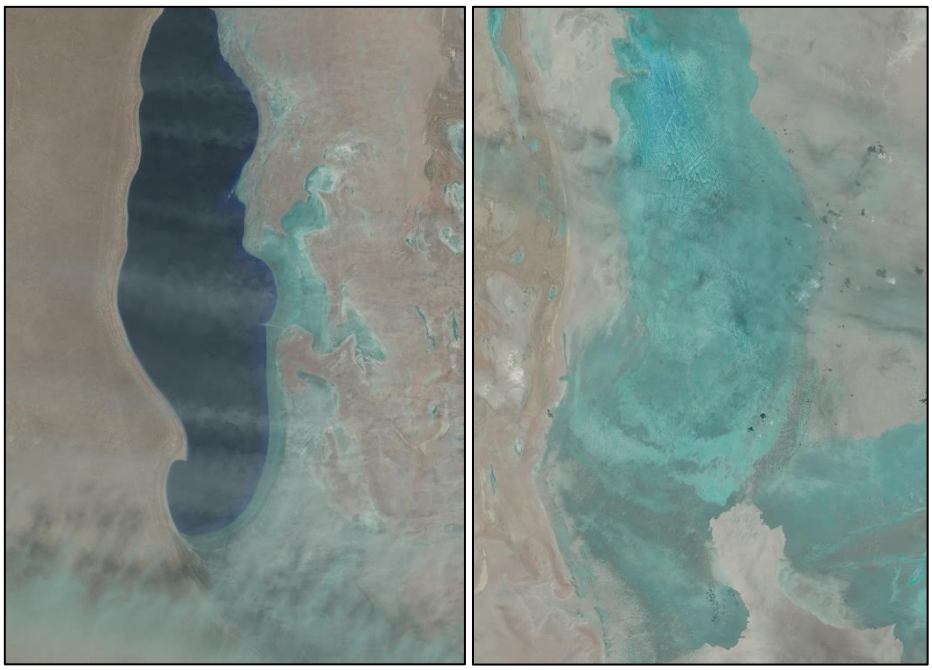

Fig.3.1 *– Two cloudy images of the Aral Sea; the first displays standard cloud cover over the area, the second displays "blue clouds" over the north of the shallow eastern basin.*

As for all satellites, malfunctions and failures are not easily correctable. This means a list of complications for satellite imagery as the cameras experience faults. The USGS keep a list of the anomalies encountered [25]. The most common found in Aral images were shutter synchronisation anomalies, specifically “caterpillar tracks” (see Fig.3.2), where the shutter is visible in the image as the image capture and shutter times fall out of alignment. While these images are correctable through Fourier transform, the removal of these lines would result in unnecessary error to those images affected.

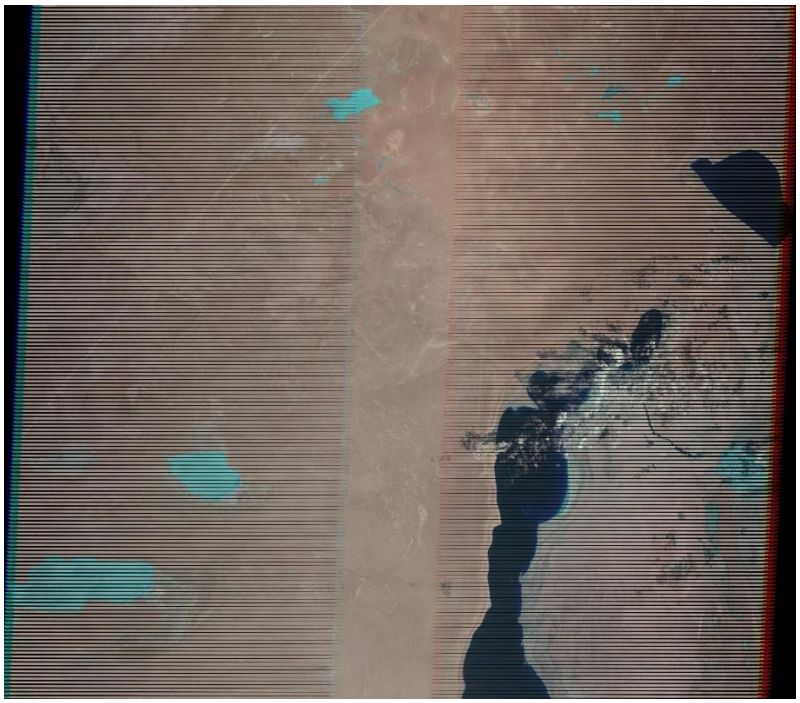

Fig.3.2 *– An anomaly present within an Aral image. These are “caterpillar tracks”.*

Over 400 individual full colour images were acquired through the Bulk Download Application. Additionally their complete image data counterparts (including all eleven wavebands and metadata) were downloaded for planned thermal analysis, but unforeseen complications induced difficulty in this analysis. Even though the majority of these images had a clear view of the sea, the edges were distorted by cloud cover; these were often to widespread to overlap images and build a full image of the Aral.

3.2. Evaporation Data

The analysis of this investigation aims to compare the extensive water loss of the Aral Sea with predicted evaporation over the same period. There are two variables that require investigation and cannot be found in textbooks; wind speed and surface temperature. Wind speed data for the Aral basin is sparse, and a complete data set was unavailable. Wind speeds in the area have largely stayed the same, unlike temperature, and therefore a basic model was constructed. A 1990 paper [26] took the average summer and winter wind speeds as $3ms^{-1}$ and $7ms^{-1}$ respectively (this value was then quoted in a 2005 book [37]); spring and autumn were between these values, and will be averaged at $5ms^{-1}$. If average wind speeds have not changed then these values can be assumed to hold true over the period of acquired images.

The temperature was to be calculate through thermal image analysis, once it had been abandoned, a new method of reaching the end goal was required. A 1999 paper [27] showed that the average surface temperature of the Aral increased by 1°C a decade, a 2001 paper [28] called the same estimate common in local temperature increases along the shoreline, and a 2013 paper [29] gave results very close to this prediction. This was modelled as a yearly temperature increase of 0.1°C from average temperatures within the 1999 article; Winter (DJF) -5.2°C, Spring (MAM) 10.9°C, Summer (JJA) 26.3°C, Autumn (SON) 10.2°C. For each succeeding year 0.1°C was added to the monthly average, for each preceding year 0.1°C was subtracted. These results are similar to the wind speed prediction as the autumn and spring values are approximately medial to the winter and summer values.

4. Analysis

4.1. Image Analysis

All downloaded images are at an angle, they are rotated to the right at approximately 10°. Initially this was believed to be a constant angle and a macro was considered for the task, however the images vary by a few degrees; the reason for this is unknown, and unspecified by the USGS, it is likely small rotations by the satellite itself. Subsequently each image had to be individually rotated using the ImageJ image processing software [30], the black surround

was then cropped away leaving only the image itself at a position 90° to the equator. The standard square crop tool was not used for these images; the Landsat satellites progress around the planet at high velocities, and are unable to produce a square image due to the change in position before the image is complete (see Fig.3.2). The images produced are parallelograms, and therefore the polygon selection was used before the cropping tool.

These images are around 7000x8000 pixels, and require a large amount of processing power to analyse and alter. Through some unfortunate restrictions on hardware performance, a small number of these images could not be processed with their original formatting. In an attempt to reduce the images to a processable size, the dimensions of the image by a small fraction (the belonging mosaic images were reduced by the same ratio). To ensure minimal loss of information, the image format was kept constant and no other performance improving changes were made.

To analyse the Aral Sea as a whole a full image must first be constructed. This mosaic was created using image editing software Paint.NET [31], which allowed for close observation in constructing the full sea, ensuring precision (see Fig.4.1). Canvas size was increased by a factor of 1.5 (approximately), to enable the entire sea to fit within the frame. Then an amalgamated image was created using geographical features of the Aral as reference points to align the satellite images. For a complete mosaic between three and six separate images of the Aral were required; the Aral can be contained within three images, but anomalies required overlapping of images for a clear view of the sea. Of the ~400 images that were acquired, only some 30 gave a clear view over the 18 day orbit. Once compiled into a single image, there are 9 usable images of the South Aral Sea (the North Aral was then removed from the investigation as it reduced the usable image count to six. All further uses of “Aral” or “Aral Sea” refer exclusively to the southern region).

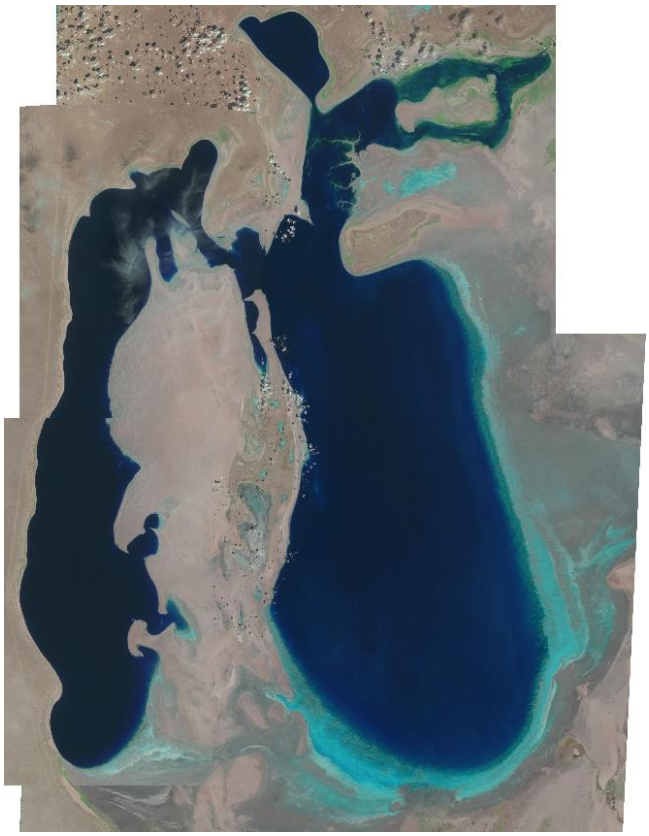

Fig.4.1 *– A full mosaic image of the Aral Sea (image: September 2002).*

The only analysing of images performed is the colour threshold. Using HSB space, this aims to remove all but the water from the mosaic images, reducing the sea itself to black, and everything else to white. All images were opened twice, using one as reference guide to ensure precision. The thresholds reduced the majority of the sea to black, resulting in an almost identical silhouette; however limits are reached and to perfect one region of the sea another begins to degrade. Close inspection is a necessity, and a compromise must be met when an area equal to that of the sea is acquired but remnants of other areas contribute to them. Each image had to be thresholded without consideration of the previously completed, as each image will require different values of Hue, Saturation and Brightness will be required.

Fig.4.2 *– An image after threshold has been performed (image: September 2002).*

4.2. Mathematical Analysis

4.2.1. Image Data Analysis

For the surface area of the Aral to be calculated, the conversion values between pixels and meters must be found. To achieve this, Google Maps [32] web based software was utilised as a measurement tool. Maps is an advanced satellite imagery software with numerous features, most relevant is the ability to connect two points on the image which maps will calculate the distance between them and convert that into meters. This allows high quality magnification to pinpoint the exact features being connected; this line was then repeated on each of the mosaic images to calculate the conversion rate between the SI distance given by Maps and the pixel separation.

However, as with all photographs, it cannot be assumed that the x and y dimensions of each pixel are equal. Therefore when the line is repeated on each image the angle is taken (any variance is a change in the entire image rotation, as the landscape does not change

position), and then trigonometric functions performed on each image to retrieve measurements of both planes. The area of each pixel is equal to the product of the x and y components. The area of the Aral Sea is thus equal to the pixel area multiplied by the number of pixels that correspond to the sea; this value was measured by the threshold performed on each of the images.

Image Date	Surface Area (km²)
(16-23)/06/1987	19,516
(15-22)/09/1989	18,508
13/03/2002	13,222
(16-23)/05/2002	12,159
(12-30)/09/2002	10,183
24/10/2011	6,072
(28/07)-(04/08)/2013	4,099
(03-12)/07/2014	3,796
(13-20)/08/2014	3,479

Fig.4.3 *– Table displaying the results of the Aral Sea surface area.*

Once the surface area of the Aral Sea had been determined, the volume can be estimated; however, a method of calculating its depth was first required. As the Aral was a vast body of water three decades heretofore, there has been little to no investigation into its large barren landscape; there are no topographical maps of the empty sea-bed available. Without data on surface configuration of the Aral's floor an exact volume measurement cannot be determined; a model is then necessary.

If the Aral is treated as a paraboloid then any inconsistent features of the terrain, such as deep crevices and the myriad of islands, can be removed and averaged into the curved declining gradient. This endows the sea with a smooth rounded basin, similar to that which many smaller lakes and rivers possess. However, the formula for calculating a paraboloids volume requires maximum depth; the maximum depth of the Aral in 2013 was 69m [33], this gives a volume considerably larger than the Aral Sea holds for the maximum depth itself is an inconsistency removed by the paraboloid.

The volume can be calculated from average depth measurements to establish an estimation over the entire course of the images, using a linear trend-line. Average depth is a scarce measurement though, so a method of calculating the values was established. A large dataset that does exist is the surface elevation of the Aral Sea relative to that of the Baltic Sea [34] (which has costal gauges used for sea level measurements due to its strong linear trends

with isostasy [35]). Under the assumption that the paraboloid is a model that closely resembles the Aral basin on a substantial scale, then any decrease in the surface elevation is an equal decrease in the average depth.

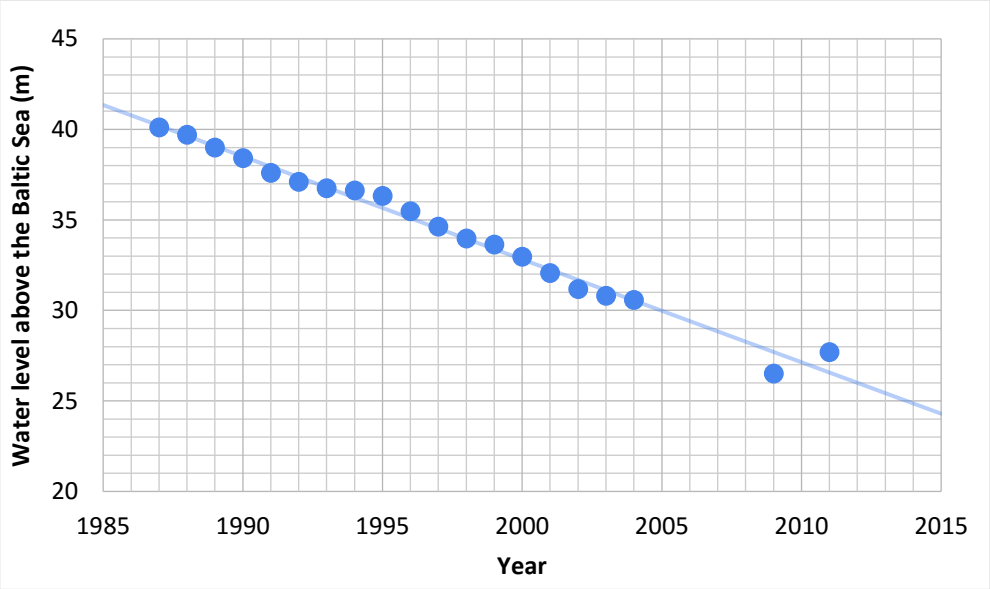

Fig.4.4 *– A graph displaying the change in surface elevation of the Aral Sea above that of the Baltic Sea, with a linear trend predicting elevation of future years.*

By taking the single average depth data points (16.1m, 1987) [33] and applying to the decline in surface elevation (1987-2004) then an estimation of the "maximum depth" of the paraboloid equation is achieved. Only two surface elevation values exist beyond 2004, while these may appear more distant from the estimated linear trend, they are responsible for allowing the trend to continue until 2014; the lower 2009 value was measured when the Aral began a final exponential decay, diverging from the predicted trend, but very heavy leading to the 2011 peak [36]. The equation then required to determine the estimated volume of the Aral Sea is:

$$V = A \times (\bar{d} - \Delta h) \quad \text{(Eq.1)}$$

By plotting these resulting values with a second order polynomial trend, a close fitting estimation of the volume between 1986 and 2015 is achieved:

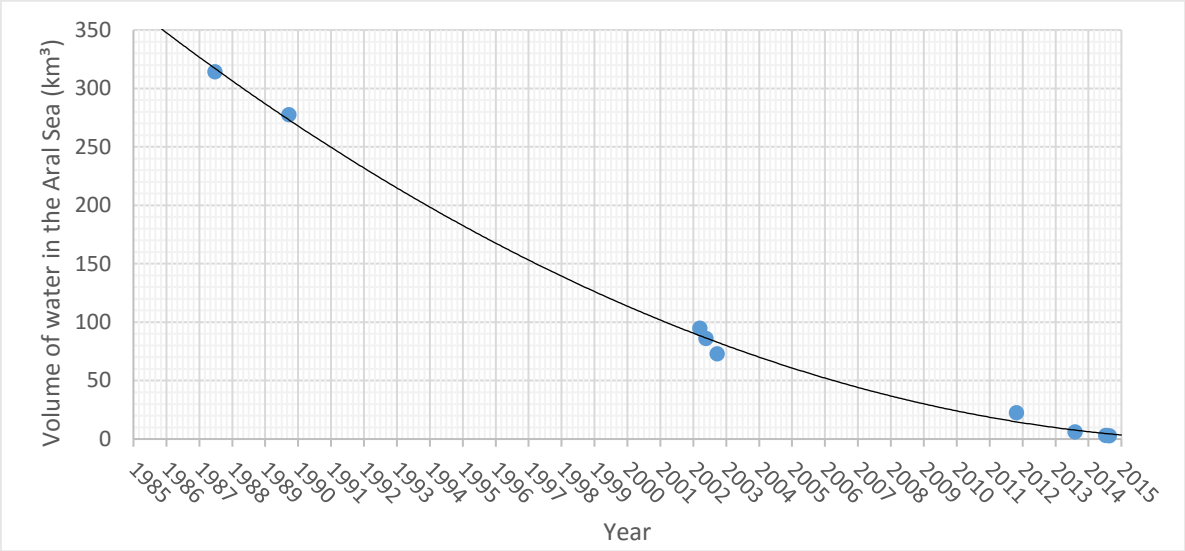

Fig.4.5 *– A graph displaying the volume of the Aral Sea for each image and a trend predicting the path of its decline.*

The equation of this trend-line is given below, by performing a derivation the rate of water loss per year can be extrapolated:

$$y = 0.323x^2 - 1304x + 10^5 \quad \text{(Eq.2)}$$

$$^{dy}/_{dx} = 0.646x - 1304$$

4.2.2 Evaporation Data Analysis

To calculate evaporation all terms present in the Shuttleworth equation must first be calculated or found; the equation is given below:

$$E_{mass} = \frac{mR_n + \gamma(6.43)(1+0.536U_2)\delta e}{\lambda_v(m+\gamma)} \quad \text{(Eq.3)}$$

Net Irradiance (R_n) is the energy given by sunlight per square meter during a day (not necessarily absorbed). The maximum radiance given is when the sun is at its zenith on a clear day, at this point the surface receives approximately 1050 Wm^{-2}. The minimal radiance given is more difficult to define; the World Meteorological Organisation claims that “sunshine” is anything over 120 Wm^{-2}, which is the approximate level on a dark and overcast day. Under

the assumption the Aral Sea region experiences an even share of both extremes (an unfortunate manifestation of the area's climate is the extreme seasonal weather it experiences), then the average radiance of the Aral can be taken as midway between these values (585 Wm^{-2}). This results in a Net Irradiance of:

$$R_n = 2.527\times10^{10} mJm^{-2}day^{-1}$$

The vapour pressure deficit (δe) is the difference between the water vapour pressure and the saturated water vapour pressure, dependant on temperature. Below 0°C it is assumed to have a value of 0, otherwise it is given by the equation:

$$\delta e = p_w - p_{ws} = \left(133.32\times10^{A-\frac{B}{C+T}}\right) - \left(\frac{e^{\left(77.345+0.0057T-\frac{7235}{T}\right)}}{1000T^{8.2}}\right) \quad \text{(Eq.4)}$$

As previously stated, the temperature (T) and wind speed (U_2) are taken from average values and modelled over the entire period of the images. Wind speed remains annually unchanging over this time, where temperature increases by 0.1°C a year resulting in the graph below:

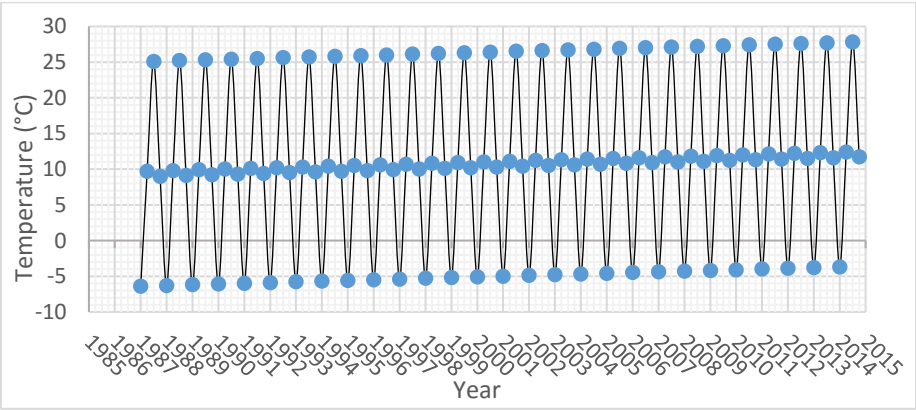

Fig.4.6 *– A graphed representation of modelled temperature change, displays yearly increase in average seasonal temperatures.*

The final elements of this equation are the latent heat of vaporisation for water, with a value of $\lambda_v = 2.257\ MJ\ kg^{-1}$, and the slope of the saturation pressure curve, which has the equation:

$$m = 0.04145e^{0.06088T} \quad \text{(Eq.5)}$$

All values for temperature and wind speed (the only two variables in the final equation) then calculated the surface evaporation in meters per year, the obtained value was consistent to 5 decimal place over the 27 years; $0.16172\ m\ year^{-1}$. This value then had to be used in calculating the volume decrease due to evaporation. To achieve this, a plot of the changing surface area was fitted with a second order polynomial trend-line (as the sea floor is an assumed smooth curve), the resulting equation was then able to predict the annual decrease in volume. Each data point corresponded to a quarter year; with the small change in depth over this short period, the angled walls of the paraboloid did not need to be considered, and each quarter was treated as though it had a regular cross-section. The sum of all yearly quarters is therefore equal to the decline in volume attributed to evaporation.

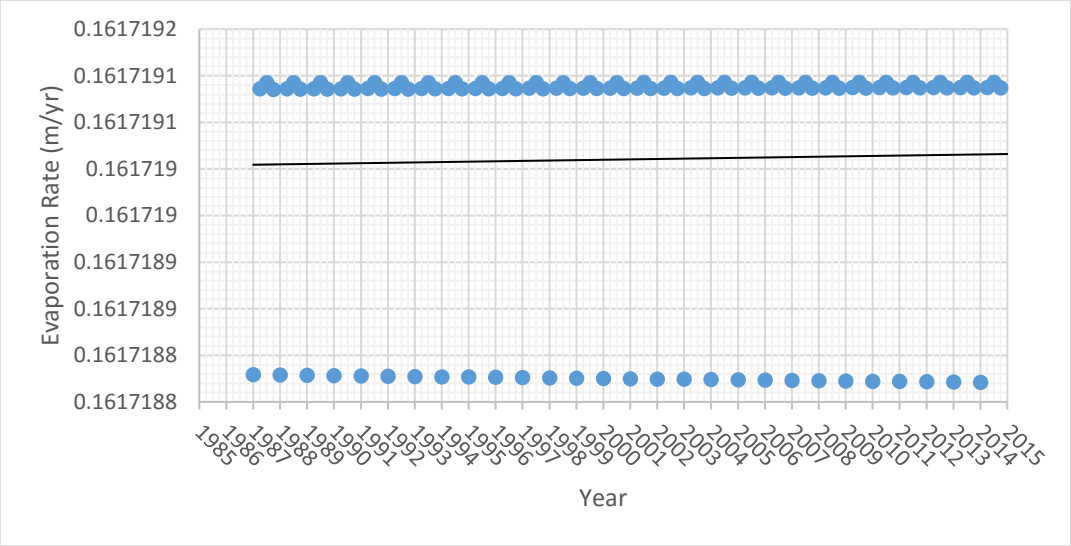

Fig.4.7 *– A graph displaying the predicted increase in evaporation rate per year, with seasonal variation and a linear trend.*

4.3. Error Analysis

4.3.1. Image Error Propagation

This is a full error analysis of all processes and assumptions made throughout the investigation. The first operations performed, rotate and crop, have errors resulting from quality loss; these are considered negligible due to the large image dimensions. This remains true for any resize procedure used, as the dimensions are reduced by a minimal amount and retain their large size.

The first errors of significance originate from the mosaic images, due to alignment and overlapping. These were experimentally measured through observation and were found to remain undetected for up to 10 pixels, following this the border inconsistency is conspicuous. A border consists of 2 images, so this gives an error of 5 pixels per image (Note: This is per image edge, each image can have 20 pixels of error over 4 dimensions). The average dimensions of each Landsat mission have similar values to each individual image and can be used for the calculation. Therefore the percentage error is given by the sum of each average dimension multiplied by 5 pixels and divided by the product of dimensions, multiplied by 100%. To obtain the percentage error of each mosaic, this value is multiplied by the number of images that assembled the mosaic:

$$\%M_{Err.} = N_M\left(\frac{2(5)(d_x+d_y)}{d_x d_y}\times 100\%\right) \quad \text{(Eq.6)}$$

The error in the threshold varies with the pixel value (0→255), as the y axis is the number of pixels for each value, therefore intensity of the error changes across the x axis. This error was once more tested through experimental observation; alternating between regions of high, low and zero y value to ascertain the general error. The outcome was that after 5 steps in the x direction a definite variance in the image could be seen, at any intensity (Note: in a region of zero intensity a variance may not be observed over 5 steps; this is inconsequential as with zero intensity there is zero change to the image). This error is consistent for Hue, Saturation and Brightness; with two selectors for each this value is halved, resulting in the equation:

$$\%Thrsh_{Err.} = 3\times\left(\frac{5}{255}\times\frac{1}{2}\right)\times 100\% = 2.94\%$$

The errors taken for pixel value calculations emerge from repeating the reference line drawn on Maps on the mosaic images. The error for angle was a consistent 1°, as this value had little variance. The error for line positioning can be defined only as the lines length, as the error angle in angle assures that it is approximately parallel. This has a fluctuating error dependant on the image dimensions; the error wavers anywhere between 5 and 10 pixels, where the line length has a minimum of ~715 pixels and a maximum of ~1450 pixels. These error values were chosen through experimental observations, after several images with

minimal length lines gave errors of 5 pixels and several of the maximal length lines gave errors of 10 pixels; the medial lines must then follow the same ratio.

The percentage error of length is equal to the error divided by the length, multiplied by 100%; this is the error of both length in pixels and the conversion length of meters/pixel. To obtain the error through a trigonometric function the derivative must be taken; the derivative must be multiplied by the error of the value within the function (Note: radians, not degrees), divided by the original function, and multiplied by 100%. This must be done for both the x and y dimensions independently, then the sum of errors is taken. This gives the error equation:

$$\%Pxl_{Err.} = \frac{\left(\frac{d(\cos\theta)}{dx}\right)\times\Delta\theta}{cos\theta} + \frac{\left(\frac{d(sin\theta)}{dy}\right)\times\Delta\theta}{sin\theta} + \Delta h \quad \text{(Eq.7)}$$

There is an insufficient amount of data acquired during this investigation to draw any errors from the paraboloid model constructed; an error cannot be estimated because no reference values of the surface or volume are considered. However, errors can be taken from the surface elevation data; taken from the difference between the plotted trend-line and the data points with the largest separation from it. This results in an error of approximately 1m; dividing by the trend estimation and multiplying by 100% gives the percentage error. The final errors in key sections are given in the table below:

Image Date	Image Error	Area Error	Volume Error
(16-23)/06/1987	5.64%	11.32%	15.07%
(15-22)/09/1989	5.10%	10.75%	14.50%
13/03/2002	3.47%	9.12%	12.87%
(16-23)/05/2002	4.00%	9.68%	13.43%
(12-30)/09/2002	4.26%	9.79%	13.54%
24/10/2011	3.46%	9.26%	13.01%
(28/07)-(04/08)/2013	3.98%	9.63%	13.38%
(03-12)/07/2014	3.98%	9.75%	13.50%
(13-20)/08/2014	3.98%	9.64%	13.39%

Fig.4.8 *– Table displaying the all significant percentage errors of this image analysis.*

Note: Each successive error includes the previous error within its calculation.

4.3.2. Evaporation Error Propagation

The evaporation equation simplifies to exact values and a few variables; consequently leaving little room for error. However, the required variables were all estimated using models built of mean values, with no consideration of the extreme. It is known that anomalous storms of up to 30 ms^{-1} can occur in the harsh winters of the Aral basin [37]. However, these storms are rare occurrences, and only occur during the three months of winter. The current wind speed average is 5 ms^{-1}; assuming no more than three day of storms (once a month) then:

$$\%U_2 = \frac{30\times3}{5\times365}\times100\% = 4.9\%$$

Net Irradiance cannot be given an exact error from absence of sufficient data; only min/max values are available and error estimation from these values would be largely overestimated and incorrect over yearly periods. The only obtained values for Aral temperature are consistent with the model produced, therefore it must be assumed accurate.

There is however one large error present in the evaporation data; the prediction of change in surface area. This data was taken from the image processing calculations, consequently the errors already present in the area calculations become errors in the evaporation. The March 2002 data point had to be removed from this estimation as seasonal changes were reducing the accuracy of the trend-line, adding additional errors. As the exact error variation is unknown, the maximum error of the area calculations will be taken as the error over the entire area decrease (as only 2% difference exists between the largest and smallest errors, this overcompensation on error will have little effect on the resulting values). The sum of wind speed error and area error gives a final evaporation error of:

$$\%Eva_{Err.} = 16.22\%.$$

5. Discussion

The calculations performed on the satellite images estimate that in the past 27 years, the volume of the Aral Sea has decreased from 314.2 km^3 to 2.8 km^3, an alarming reduction of 311.4 km^3. Once error analysis is considered, the less distressing scenario of 263.7 km^3 decline is an inappreciable improvement. In contrast, the approximation of evaporation since 1987 is 60.8 km^3, again considering error analysis the maximum value for evaporation is 70.7 km^3. This therefore leaves a minimum of 193 km^3 of water unaccounted for by the climate change in the area.

5.1. Discussion of Evaporation

Is it correct to assume that the models and techniques utilised in this investigation sufficient in drawing this conclusion? This question requires another glance at each piece of the methods used. The temperature calculation, as previously noted, was originally meant to be drawn from thermal image analysis. This analysis involved using the programming language R to compile a piece of code [38] that would read the metadata file of a Landsat image and employ all 11 spectral bands to extract the brightness temperature (using equations given by the USGS [39]. From these thermal maps an average value of the Aral temperature could have been calculated; however only 9 images were in use by the end of the investigation, giving a very small sample on a value with large yearly fluctuation.

The temperature model constructed during this investigation has the absence yearly fluctuations, leading to a deviation from the true values across many seasons; it retains the benefit of being the correct average increase however, even though yearly increases contain discrepancies. While this may cause small errors in the temperature, the evaporation rate was correct to 5 decimal places with a 2.7°C increase over 27 years; it is likely that any fluctuations would not have had significant impact in the evaporation rate, therefore the temperature model is valid.

The wind speed estimation is based on average values taken over 18 years, however wind speed in the area has significantly larger variation than temperature. It is known that the western shore experiences far greater winds than the other regions, however no values for

these are given. The only other value is the large winter storms endured by the sea, which do provide a significant error within the model. All average values are calculated from the coastal regions of the sea, the wind speeds over the vast majority of the sea remain uncalculated. While these do remain average values, their validity over a number of years remains unknown. The true validity of this model requires further investigation.

One aspect of evaporation that was disregarded was the increasing levels of salinity in the Aral's waters. This salinity is a major contributor to the local climate change and other destructive effects in the region. Tens of thousands of tonnes of salt are carried away from the basin every day, eliminating any chance of crops surviving in local soils. Salt water evaporates at a lesser rate than its fresh water counterpart, and therefore increases the separation between the volume lost and the volume evaporated.

5.2. Discussion of Images

The image analysis performed during this investigation is credible; each operation has its precision defined by its error. There are improvements to be made on the precision; for an ideal satellite image mosaic, each image should be further analysed prior to amalgamation. This is because the gain will vary between image, returning incorrect intensities and true colour may be skewed; this is far more obvious in mosaics of individual spectral bands, where intensities cause far larger deviations in the greyscale values. While this has lesser impact on the full colour thresholds, for any further extensive investigation into the topic, the alteration may be a necessity.

Greater improvements on the threshold could also be made; to remove cloud cover and degradation of some regions (possibly due to gain), the threshold technique should be abandoned. Outlining the sea's coast (including islands) would result in greater accuracy, as no compromise would have to be met. Once the coastline has been highlighted, the entire area within its borders (excluding islands) could be reduced to black, giving the equivalent threshold image; in contrast to the threshold, this image would contain no error from clouds, and could subsequently use images with far greater cloud cover.

The area calculation is yet another credible set of data, it has no error of its own, but the sum of all previous errors are present at ~10%. The largest of these is from the calculation of the individual pixel dimensions; through using Google Maps as a reference which does not have the precision desired for many investigations. There are various mapping softwares (including Google Earth) that allow images to be overlaid on maps; this would allow a precise conversion for the Aral with a measurement only being taken once (no repeating a line). The precision of Googles Maps pixel to distance conversion is sufficient for this investigation.

Treating the Aral Sea as a paraboloid as an estimation of volume is not a perfect model. With additional data on average depth across different regions of the sea, such as costal depths and the depth of the large flat plains of the sea floor, then this has the potential to be crafted into a tenable approximation. With the current data available, this still stands as a rational estimation, and the error margins (~14%) are of adequate proportion to maintain accuracy. The only flaw present within this model is the assumption that sea elevation change is equivalent to the change in average depth; while this may hold true for a smooth paraboloid, the Aral is merely being modelled as such. A correction to this omission would be further investigation into any existing average depth measurements.

5.3. Further Discussion

Naturally, the most beneficial data to the volume calculation that future investigations could measure, would be a topographical map created from study of the largely barren basin. From this, a realistic three dimensional model of the Aral's features, and subsequently their relationship to the volume, could be established. Coupled with the previously suggested revisions to the threshold and pixel dimension calculation, this improved model could yield a veracious result to the decline in the volume of the Aral Sea.

I would recommend future research make use of all available thermal image data and retrieve surface temperature values from images over extended periods; then a precise model taken from observed temperatures can be built, in preference of using average temperatures and temperature change estimates. Additionally, any analysis aiming to have a definite value for evaporation must have an abundance of data on the local wind changes; although only a

very large data set requires this, as individual changes in temperature and wind speed, even at extreme values, have little outcome on the final evaporation volume.

This investigation has been compelled to make some assumptions that decrease the validity of its results. The deficiency of statistics into the Aral Sea is astounding, with almost all articles written by a few familiar names. With further analysis these methods could return results of a higher precision, with the models used taking results from much larger sets of data. There is plentiful data from the 1990's, relative to other times, but data of the past 10 years is scarce. New data on the continuously changing situation would be a large asset in ascertaining the decline in volume, and the volume that relented to evaporation, to a far higher precision.

The errors in this investigation are of a justifiable percentage, when the number of large errors present is considered; no value experiences a significant change after its error margins are reviewed. The errors in this analysis have arguably been a beneficial asset; the large error margins display that even in the scenario of lowest value of volume, highest value for evaporation, there is still a vast loss of volume above that lost to evaporation. In essence, the error values of the results aid in negating the uncertainty left by incomplete models and assumptions.

6. Conclusion

This investigation used Landsat satellite imagery to predict the surface area of the Aral Sea through a threshold. By modelling the Aral as a paraboloid (under the assumption its terrain could be evenly smoothed to the average depth) an estimation of volume was calculated and further used to explore the volume reduction. By then calculating the evaporation using a model built on average temperature and the approximation of its steady increase (also using a model of wind speed with reduced validity), the two sets of data can be compared, and a deduction of the data made. Hypothetically, this investigation can be utilised in the future as basis for improved methods and models for a higher precision result.

The results obtained by this investigation highly suggest that climate change in the Aral Sea region is not wholly responsible for the extensive volume of water lost. While it is a well-

established fact that irrigation canals built by the former USSR are a significant factor, if not entirely responsible, for the destruction of the Aral Sea, this investigation provides insight into the water loss that can be directly linked to the irrigation and not a causal factor of the canals. An estimated 250 km^3 of water was lost from the Aral Sea through a means other than evaporation; while irrigation can remove a significant volume of water, it usually remains within the same regional water cycle. Therefore this investigation concludes that approximately 250 km^3 of water drained from the Aral Sea was lost to the ground through poorly constructed irrigation canals.

7. References

[1] CRACKNELL, A.P. and HAYES, L. Introduction to remote sensing. 2nd ed. CRC Press. 2007.

[2] Sandau, R. Digital Airborne Camera: Introduction and technology. Springer. 2010

[3] KIDDER, S.Q. and VONDER HARR, T.H. Satellite meteorology an introduction. UK ed. Academic Press, 1995

[4] NASA, 2013. History (Landsat) [online]. NASA. Available at: http://landsat.gsfc.nasa.gov/?page_id=2281 [Accessed 29 October 2014]

[5] Cracknell, A. and Hayes, L. Op. cit. p.5

[6] CHELTON, D.B. and WENTZ, F.J. Global microwave satellite observations of sea surface temperature for numerical weather prediction and climate research. *Bulletin of the American Meteorological Society,* 2005, 86(8), pp.1097-1115

[7] NRO, 2014. Available at: http://www.nro.gov/ [Accessed 29 October 2014]

[8] USDA Forest Service, 2014. Remote Sensing Applications Center. Available at: http://activefiremaps.fs.fed.us/ [Accessed 29 October 2014]

[9] RICHARDS, J.A. and JIA, X. Remote sensing digital image analysis. 3rd ed. Springer. 1998.

[10] NASA, 2013. Landsat 8 instruments [online]. NASA. Available at: http://www.nasa.gov/content/landsat-8-instruments [Accessed 29 October 2014]

[11] NASA, 2013. Landsat 8 bands [online]. NASA. Available at: http://landsat.gsfc.nasa.gov/?page_id=5377 [Accessed 29 October 2014]

[12] CRACKNELL, A.P. The advanced very high resolution radiometer. Taylor & Francis. 1997.

[13] NASA, 2013. The worldwide reference system [online]. NASA. Available at: http://landsat.gsfc.nasa.gov/?p=3231 [Accessed 29 October 2014]

[14] USGS, 2014. FAQ about the Landsat missions [online]. USGS. Available at: http://landsat.usgs.gov/tools_access_all_faqs.php [Accessed 29 October 2014]

[15] PRAVALIE, R., SIRODOEV, I., PEPTENATU, D. Detecting climate change effects on forest ecosystems in southwestern Romania using landsat TM NDVI data. *Journal of Geographical Sciences*, 2014, 24(5), pp.815-832.

[16] Lee, M. and Jung, H.S. Analysis on the snow cover variations at Mt. Kilimanjaro using Landsat satellite images. *Korean Journal of Remote Sensing,* 2012, 28(4), pp.409-420.

[17] USGS, 2014. Aral sea [online]. USGS. Available at: http://earthshots.usgs.gov/earthshots/sites/all/files/earthshots/1977%20cropped%20full%20mosaic.png [Accessed 29 October 2014]

[18] NASA, 2011. Aral sea [online]. Available at: http://eoimages.gsfc.nasa.gov/images/imagerecords/52000/52002/aralsea_tmo_2011227_lrg.jpg [Accessed 29 October 2014]

[19] PRYDE, P.R. Environmental management in the Soviet Union. Cambridge University Press. 1991.

[20] GLANTZ, M. Creeping environmental problems and sustainable development in the Aral Sea basin. Cambridge University Press. 1999.

[21] KHARIN, N. Vegetation degradation in central Asia under the impact of human activities. Springer. 2002.

[22] MICKLIN, P.P. Disiccation of the Aral Sea: a water management disaster in the Soviet Union. *American Association for the Advancement of Science,* 1988, 241(4870), pp.1170-1176

[23] MICKLIN, P.P. The Aral Sea crisis and it's future: an assessment. *Eurasian Geography and Economics*, 2006, 47(5), pp.546-567.

[24] USGS, 2014. Earth Explorer [online]. Available at: http://earthexplorer.usgs.gov/ [Accessed 12 March 2015]

[25] USGS, 2013. Anomalies [online]. Available at: http://landsat.usgs.gov/science_an_anomalies.php [Accessed 12 March 2015]

[26] BORTNIK, V.N. and CHISTYAEVA, S.P. Gidrometeorologiya i Gidrokhemiya Morei SSSR. *Gidrometeoizdat*, 1990, 7(Aral'skoye more).

[27] SMALL, E.E., CIRBUS SLOAN, L., HOSTETLER, S., GIORGI, F. Stimulating the water balance of the Aral Sea with a coupled regional climate-lake model. *Journal of Geophysical Research,* 104(D6), pp.6583-6602.

[28] SMALL, E.E., CIRBUS SLOAN, L., NYCHKA, D. Changes in the Surface Air Temperature Caused by the Desiccation of the Aral Sea. *Journal of Climate,* 2001, 14(3), pp.284-299.

[29] GINZBERG, I., KOSTYANOY, A.G., SHEREMET, N.A. Thermal Conditions in the Aral Sea (1982-2000) from Satellite Data. *Mapping Sciences and Remote Sensing,* 2013, 40(4), pp.231-241.

[30] National Institute of Health, 2004. ImageJ [online]. Available at: http://imagej.nih.gov/ij/ [Accessed 12 March 2015]

[31] dotPDN LLC, 2014. Paint.NET [online]. Available at: http://www.getpaint.net/index.html [Accessed 12 March 2015]

[32] Google Inc., 2015. Google Maps [online]. Available at: https://www.google.com/maps/ [Accessed 12 March 2015]

[33] MICKLIN, P., ALADIN, N., PLOTNIKOV, I. The Aral Sea: The Devastation and Partial Rehabilitation of a Great Lake. Springer. 2014

[34] KOSTIANOY, A.G. and KOSAREV, A.N. The Handbook of Environmental Chemistry: The Aral Sea Environment. Springer. 2010

[35] ZORITA, E. and HÜNICKE, B. Is the Baltic sea-level change accelerating?. *EGU General Assembly 2010,* pp.14078.

[36] CRÉTAUX, J.F., CALMANT, S., KOURAEV, A. Lake Studies from Satellite Altimetry. Springer. 2010.

[37] ZAVIALOV, P.O. Physical Oceanography of the Dying Aral Sea. Springer. 2005.

[38] R-Bloggers, 2015. Landsat thermal code [online]. Available at: http://www.r-bloggers.com/landsat-thermal-imaging/ [Accessed 10 March 2015]

[39] USGS, 2013. Using the Landsat 8 Product [online]. Available at: http://landsat.usgs.gov/Landsat8_Using_Product.php [Accessed 12 March 2015]

[40] DOUGHERTY, T.C. and HALL, A.W. Environmental impact assessment of irrigation and drainage projects. Food and Agriculture Organisation of the United Nations. 1995.